

Peeling of Polydimethylsiloxane Adhesives : the Case of Adhesive Failure

Claude VERDIER^{(1)*}, Guillaume RAVILLY⁽²⁾

(1) Laboratoire de Spectrométrie Physique
CNRS and Université de Grenoble UJF (UMR5588)
BP 87, 140 Avenue de la Physique
38402 Saint-Martin d'Hères cedex
France

(2) Laboratoire de Rhéologie
1301 rue de le piscine
CNRS, UJF-INPG (UMR5520)
BP53, 38041 Grenoble cedex 9
France

ABSTRACT

The adhesion properties of high molecular weight Polydimethylsiloxane adhesives are measured using 90°-peel adhesion tests, in the high velocity range. Such adhesives undergo mainly adhesive failure in this regime. The influence of viscosity (non-Newtonian), adhesive thickness, peeling velocity, and backing properties are studied, and new unexpected behaviours are shown. The role of rheology and peeling velocity can be explained by an extension of a model already presented for cohesive failure, by using a power-law fluid for the adhesive. On the other hand, the influence of the backing rigidity reveals to be coupled with the adhesive elastic properties, this effect being correlated to the introduction of a new parameter in the model, the Weissenberg number for viscoelasticity.

Keywords : adhesion, interfaces, thin films

* Correspondence to: C. Verdier (E-mail: verdier@ujf-grenoble.fr)

INTRODUCTION

The adhesive properties of pressure-sensitive adhesives (P.S.A.) have been studied by a large number of researchers over the years, using different methods for predicting adhesive failure in particular using peeling tests^{1,2} and probe-tack tests^{3,4} but also other various approaches such as the JKR (Johnson-Kendall-Roberts) technique⁵. Prediction of the adhesive properties in terms of interfacial and rheological properties is still a challenge, and although several studies already focused on such correlations⁶⁻⁹, there is still a lack of prediction of the effect of such properties as well as geometrical effects. Recently, model polymers (Polydimethylsiloxanes, PDMS) were used¹⁰ to investigate the peeling properties of Newtonian adhesives. Although this analysis was found to predict well experimental data, it was only obtained in a rather limited range of velocities which corresponds to two-dimensional adhesive flow of the cohesive peeling branch. Indeed, previous studies reported on the complex flow behaviour of the adhesive in both cohesive and adhesive regimes, close to the peeling front^{2,11}. After a certain threshold velocity is reached, both cohesive and interfacial flow or deformation regimes show the appearance of instabilities leading to three-dimensional deformations corresponding to stable regimes for the energy release rate G (N/m) or Force per unit width ($G = \frac{F}{b}$, F is the force required to peel the adhesive strip, and b is the adhesive strip width).

To model the effect of the adhesive and rheological properties on the energy release rate G , several studies^{12,13,14,15} focused on the possible decomposition of G into the product of two different terms, W_a , the Dupré adhesion energy, and a rheological parameter $\phi(V)$ to be determined. $\phi(V)$ contains the viscoelastic contribution of the adhesive in terms of rheological

properties and the velocity of peel V , and is intimately related to the rate dependence of the microscopic motions of elements (polymer chains, networks, particles, etc.), within the adhesive :

$$G = W_a \phi(V) \quad (1)$$

It has been a source of interest to try to model this function, which can be assumed to contain both shear and elongational deformation types. Still the use of the Dupré energy of adhesion in formula (1) is under debate and might be related to more complex microscopic phenomena, due to the presence of polymer chains of different molecular weights M_w for example¹³. Finally, the geometry of the system plays a role which renders the use of (1) difficult.

In the present work, we pay attention to the adhesive (interfacial) regime of failure in a 90°-peel test and try to analyse the effect of the governing parameters, i.e. the adhesive thickness, the velocity of peel, the influence of the backing rigidity as well as the rheological adhesive properties. In the first part, experimental results are presented¹⁶, illustrating the dependence of the energy release rate as a function of the governing parameters described above. The interfacial parameters are also described and their importance is mentioned in terms of interfacial energies, determined through wetting measurements. In the second part, an explanation is proposed through the use of a power law fluid, which is typical of the PDMS adhesive used in this study. The model predicts fairly well the importance of the governing parameters in terms of the peeling velocity. To explain these results further, a new explanation is proposed in the last part, accounting for the viscoelasticity effects which appear in the high velocity regime where adhesive failure occurs. Dimensionless numbers are introduced through an empirical model. The model is in good agreement with the experimental data and might be used for other systems.

The transition from cohesive to adhesive mode of failure is also discussed.

EXPERIMENTAL MEASUREMENTS

Experimental set-up and adhesive properties

In a previous study¹⁰, model PDMS adhesives have been investigated using a peeling experiment. The set-up has been already described and is briefly recalled here. An adhesive is coated thanks to a blade coating system (thickness in the range 30-400 μm) onto an initially treated backing. In the present study, different backings are used (stainless steel of different thicknesses, 10 μm and 20 μm , and PolyEthylene-Terephthalate PET, 23 μm). After the coating is achieved, the system is rapidly set into contact with the substrate, i.e. a High density Polyethylene (HDPE). This system was selected because it enables to obtain adhesive failure at the polymer-substrate interface which is required for practical applications. The peeling system consists of two micrometric tables X and Z moving at the same velocity V, this enabling to obtain a fixed point for observations of the peeling front^{2,7,8}. The adhesive strip (adhesive and backing) is attached on the force transducer located on the vertical micrometric table moving in the Z-direction with velocity V. The substrate is located in the X-Y plane and moves in the X direction with velocity V. The whole set-up is located in a controlled chamber (fixed temperature $T=20^{\circ}\text{C} \pm 0.1^{\circ}\text{C}$, and relative humidity $10\% \pm 2\%$). As the experiment is started, corresponding to simultaneous motion of the two micrometric tables, a transient regime is found which will lead to a stable regime after a certain time, depending on the geometry as well as the viscoelastic parameters of the adhesive.

The adhesive which was selected is a long molecular weight linear PDMS (Rhodia silicones, 47V 2500,000), its zero-shear viscosity is $\eta_0=2500 \pm 100$ Pa.s and its surface tension $\gamma= 21 \pm 1$ mN/m at 20 $^{\circ}\text{C}$ (measured by the pendant drop technique, Digidrop GBX, France). A more complete rheometrical study¹⁷ (rotational rheometer RMS, cone-plate geometry) shows the following shear-rate dependence for this polymer (figure 1):

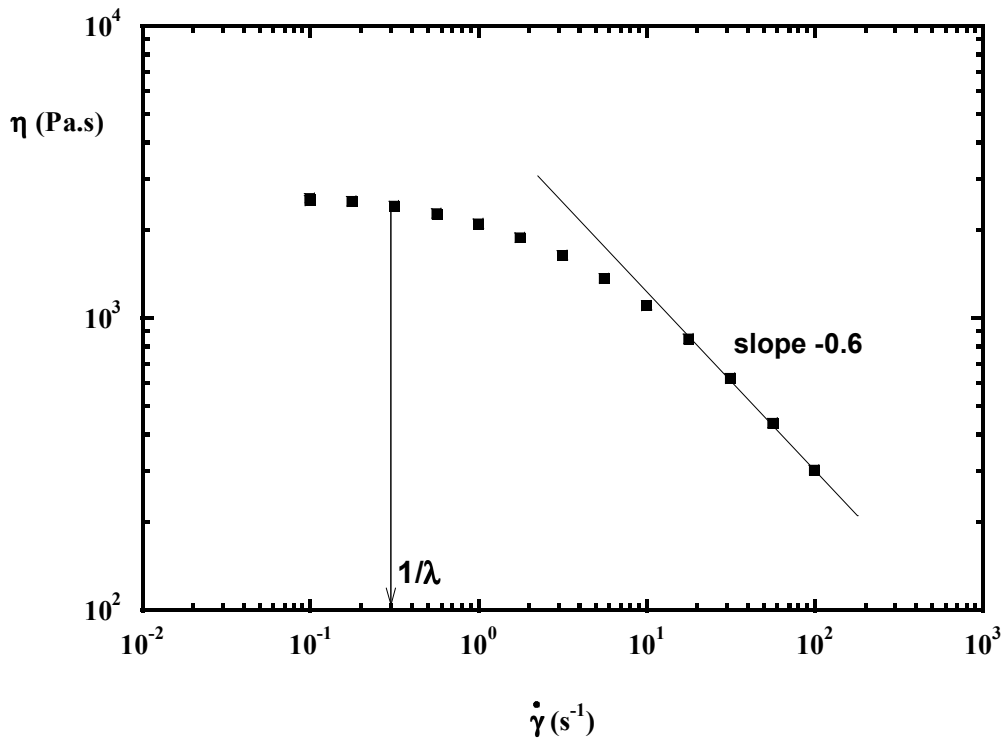


Figure 1. Shear rheometry of the PDMS adhesive polymer ($T= 20\text{ }^{\circ}\text{C}$). Determination of the longest relaxation time of the polymer gives approximately $\lambda = 3\text{ s}$.

This polymer has the advantage to present a large viscosity, followed by a strong shear-thinning behaviour at high shear rates, and to exhibit viscoelastic effects when the time scales are smaller than the relaxation time λ , which is the case (as will be shown later) for high peeling velocities. λ , the longest relaxation time, can be found at the onset of decrease on the viscosity curve (figure 1), corresponding to a critical shear rate of about 0.3 s^{-1} , therefore $\lambda = 1/0.3 \approx 3\text{ s}$.

The elongational properties of such a polymer have not been measured here, but do not exhibit strain hardening¹⁸. This behavior was shown when pulling a PDMS sample at constant stretch rate (Ref. 18, stretch rates from 0.03 s^{-1} to 3 s^{-1}). The transient elongational viscosity undergoes a slow increase followed by a plateau (defining the elongational viscosity), but shows no strain

hardening effects. On the contrary, hardening has been observed when using branched polydimethylsiloxanes¹⁸ at the highest velocity rates (around 3 s⁻¹).

When peeling is achieved, at the smallest velocities, cohesive failure is possible, but the most general behaviour corresponds to interfacial failure, i.e. the adhesive is being detached from the substrate.

Surface energy measurements and surface treatment

In order to obtain the desired peeling regimes, different backings were used and only one substrate (HDPE). The free surface energies of all materials were determined following wetting measurements using the contact angle technique coupled with a visualization technique (Digidrop, GBX, France). Fluids with known surface energy components were used. Two kinds of free surface energies decompositions were used, the one based on the Owens-Wendt¹⁹ decomposition, as in equation (2)_a, and the second one - equation (2)_b - based on the acido-basic concept by van Oss et al.²⁰ (Lewis concept):

$$\gamma = \gamma^D + \gamma^P \quad (2)_a$$

$$\gamma = \gamma^{LW} + \gamma^{AB} \quad (2)_b$$

where the surface tension γ has two components, a dispersive one (γ^D) and a polar one (γ^P) in the first case, and a Lifshitz-van der Waals (γ^{LW}) one and an acido-basic component (γ^{AB}) in the second case. The γ^{AB} component (acido-basic) is defined in terms of the electron donator (Lewis base, γ^-) or acceptor (Lewis acid, γ^+) character of the fluid or solid and is written as $\gamma^{AB} = 2\sqrt{\gamma^+\gamma^-}$.

This leads to the Dupré adhesion energy expression W_a given by :

$$W_a = \gamma_L (1 + \cos\theta) = 2\sqrt{\gamma_L^D \gamma_S^D} + 2\sqrt{\gamma_L^P \gamma_S^P} \quad (3)_a$$

$$W_a = \gamma_L (1 + \cos\theta) = 2\sqrt{\gamma_L^{LW} \gamma_S^{LW}} + 2\sqrt{\gamma_L^+ \gamma_S^-} + 2\sqrt{\gamma_L^- \gamma_S^+} \quad (3)_b$$

where θ is the wetting angle between the drop (L) and a substrate (S), and γ_L is the liquid surface tension. The surface tension or free energy components of the liquids and the solids are denoted with a subscript L or S respectively, and the superscripts LW and AB are used for the van Oss decomposition²⁰, whereas D and P are used for the Owens-Wendt method¹⁹.

Four different liquids were used for the study, water, glycerol, formamide, and diiodomethane. They span the whole range of fluids going from dispersive to polar liquids, which is useful in particular for the first decomposition (Owens-Wendt). Their components, as described previously^{19,20}, are shown in Table 1:

Liquids	γ_L	Acido-basic ²⁰			Polar-dispersive ¹⁹	
		γ_L^{LW}	γ^+	γ^-	γ^P	γ^D
Water	72.8	21.8	25.5	25.5	51	21.8
Glycerol (99% pure)	64	34	3.9	57.4	30	34
Formamide (99.5% pure)	58	39	2.3	39.6	19	39
Diiodomethane (98% pure)	50.8	50.8	0	0	0	50.8

Table 1 : **Liquid components as given by van Oss et al.²⁰ and Owens-Wendt¹⁹ (mN/m).**

Contact angles have been measured for each liquid on the two different backings (stainless steel and PET) and also for the HDPE substrate. Table 2 gives the values of the Dupré adhesion energies between a substrate and the PDMS adhesive, obtained using the two methods of decomposition, and follow equations (3)_a and (3)_b.

	γ_s (van Oss et al.)	γ_s (Owens-Wendt)	W_a (van Oss et al.)	W_a (Owens-Wendt)
HDPE	37.7 ± 2.1	38.2 ± 2.3	54.1 ± 3.1	51.9 ± 2.8
stainless Steel	59.1 ± 3.2	56.2 ± 3.4	57.3 ± 3.3	54.3 ± 3.4
PET	49.7 ± 2.7	45.5 ± 2.7	59.5 ± 3.5	55.7 ± 3.2

Table 2 : Free energies γ_s (mN/m) and Dupré adhesion energies W_a (mN/m) using the two methods.

From these measurements, it appears that the PDMS adhesive is more likely to develop affinities with respect to Stainless steel and PET, as compared with the substrate (HDPE). This is for this reason that such a substrate and backings were used. In fact, to obtain such data, we also had to use a primer for increasing the adhesion towards the PET backing. The primer which was used (typical thickness 20 μm , using a blade coating system) is an industrial one, containing acrylic copolymers filled with titanium dioxide and chloride charges. Its main effect is to increase surface roughness of the PET backing, as shown in figures 2a and 2b.

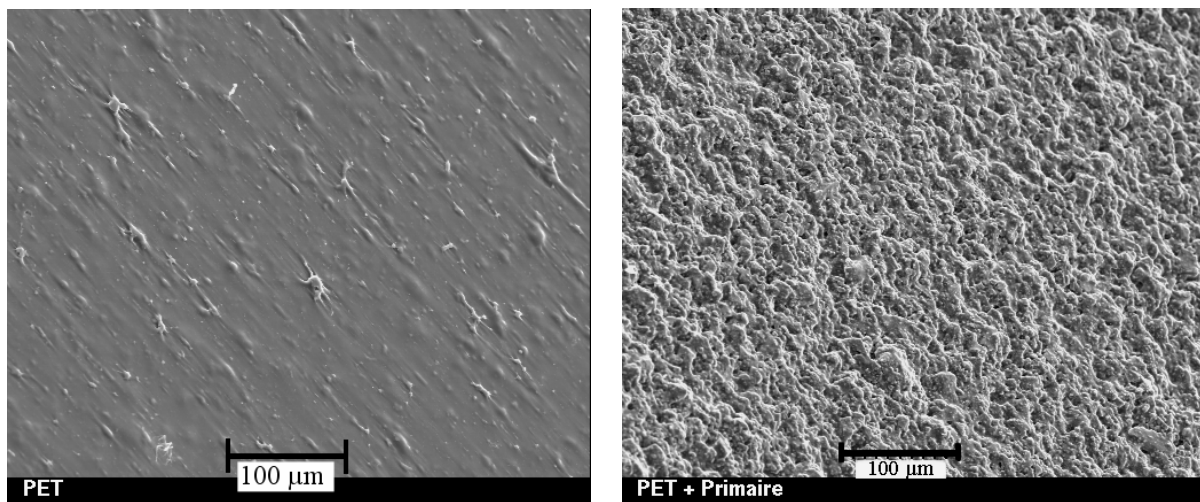


Figure 2. PET surface visualized with a SEM (X200). a) before treatment b) after treatment

The roughness is clearly increased by etching, as seen on the SEM photograph corresponding to the PET surface, after the primer was used.

To summarize this analysis, the systems used will tend to be in favour of an adhesive regime of failure at the interface between the adhesive and the HDPE substrate, and this is what is discussed next.

Peeling experiments

The peeling measurements were obtained at $T=20^\circ\text{C}$ using the peeling experiment described above¹⁶. The influence of the following parameters has been studied: adhesive thickness, peeling velocity and backing rigidity. In figure 3, we present the peeling properties of the PDMS adhesive coated onto the HDPE substrate.

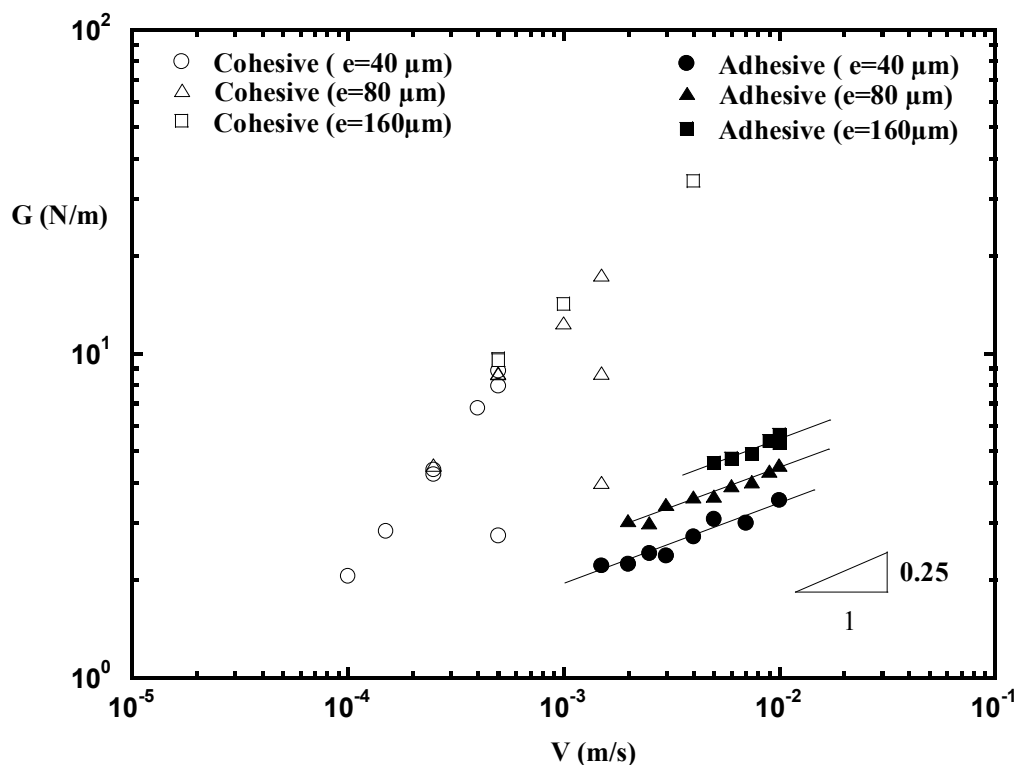


Figure 3. Peeling curve. Influence of the peeling velocity and adhesive thickness ($T= 20^\circ\text{C}$, PET backing). Cohesive to adhesive failure transition corresponds to changing from open to filled symbols

As can be seen, the rate of restitution of energy $G = \frac{F}{b}$ is plotted as a function of the peeling velocity at different adhesive thickness (e). A first regime corresponding to cohesive failure is first observed, governed by three-dimensional motion of the adhesive at the peeling front. The mechanisms associated with this regime correspond to the formation of regularly spaced filaments, as observed previously for uncross-linked PSAs^{2,7}. This is shown in figure 4a, and verified for different adhesive thicknesses (40-160 μm). The transition between cohesive and adhesive regimes occurs at a certain critical velocity V_c and will be discussed in the final part.

We will now pay more attention to the second regime, appearing in the velocity range $0.1 \text{ cm/s} < V < 1 \text{ cm/s}$, i.e. the adhesive (or interfacial) regime of failure. Again, the mechanisms of peeling are shown in figure 4b. They correspond to two-dimensional flow or deformation, the adhesive being stretched until it releases its bonds at the substrate-adhesive interface.

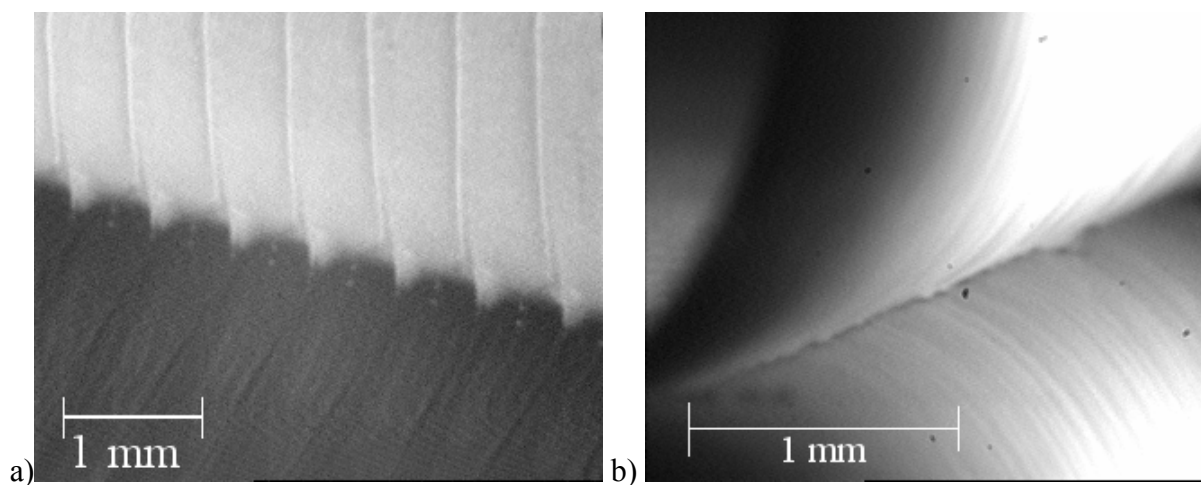


Figure 4. Photographs of the peeling front (PET backing, adhesive thickness $e=80 \mu\text{m}$).

a) cohesive failure with formation of regularly spaced filaments, $V=0.1 \text{ cm/s}$.

b) adhesive two-dimensional peeling regime, $V=0.75 \text{ cm/s}$.

This regime seems to exhibit a typical slope of 0.25 (log-log scale) in terms of the velocity, thus showing a rather slow change with peeling velocity. Figure 5 is deduced from these experiments and shows the influence of adhesive thickness for three different velocities. The change in the

slope (log-log scale) is typical of a power law relationship with index 0.33, in this velocity range and for this kind of adhesive and backing.

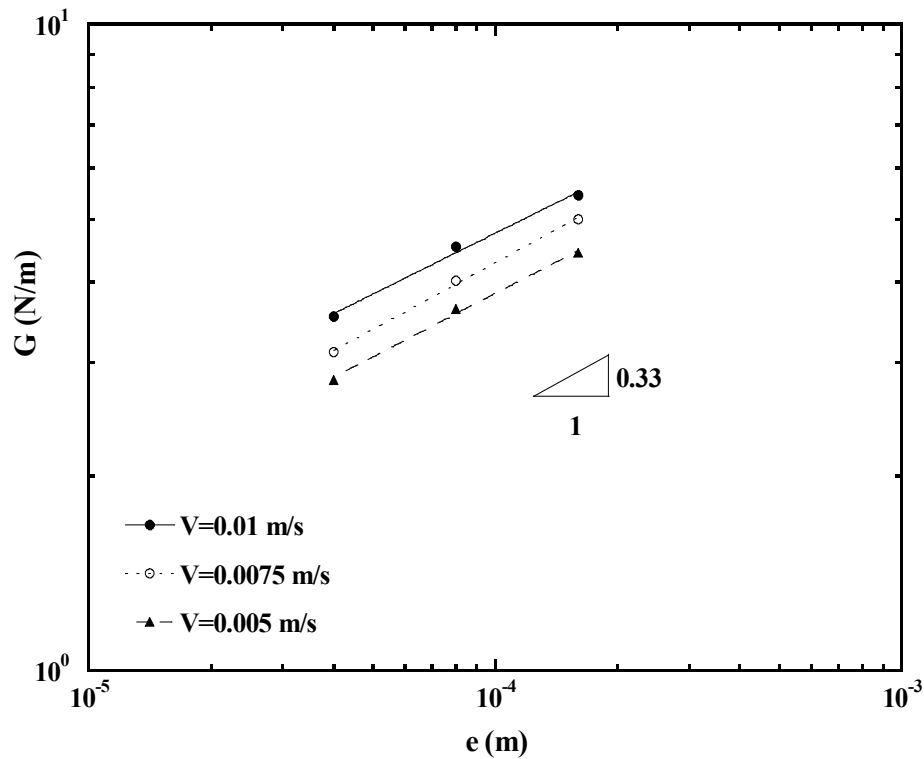


Figure 5. Influence of the adhesive thickness for different velocities ($T= 20$ °C, PET backing)

Finally, we present the variations of the energy restitution rate as a function of velocity, using different backings. Two stainless steel strips have been used, showing different thickness ($2h=10\mu\text{m}$ or $20\mu\text{m}$), as well as a PET pre-treated backing (see previous part). The important parameter is the product of the backing Young's modulus E by the momentum of inertia I (from beam theory), as shown previously¹⁰.

The characteristics of the three backings ($2h$ and $E I$) used are given in Table 3.

Backing type	Thickness (2h)	Rigidity (EI)
PET	23 μm	$3.8 \cdot 10^{-7} \text{ Pa}\cdot\text{m}^4$
stainless Steel	10 μm	$1 \cdot 10^{-6} \text{ Pa}\cdot\text{m}^4$
stainless Steel	20 μm	$7.1 \cdot 10^{-6} \text{ Pa}\cdot\text{m}^4$

Table 3 : Different backing characteristics. E is Young's modulus, $I = \frac{2bh^3}{3}$, b=strip width, 2h=backing thickness

The peeling curves of the different strips, corresponding to the three backings are shown in figure 6. Again, the velocity dependence is the same (typical slope 0.25) for the three adhesive strips. Only in the case of the Polyester backing (PET), a cohesive branch was obtained at the lower velocities, whereas in the other cases, the only regime observed is the interfacial one.

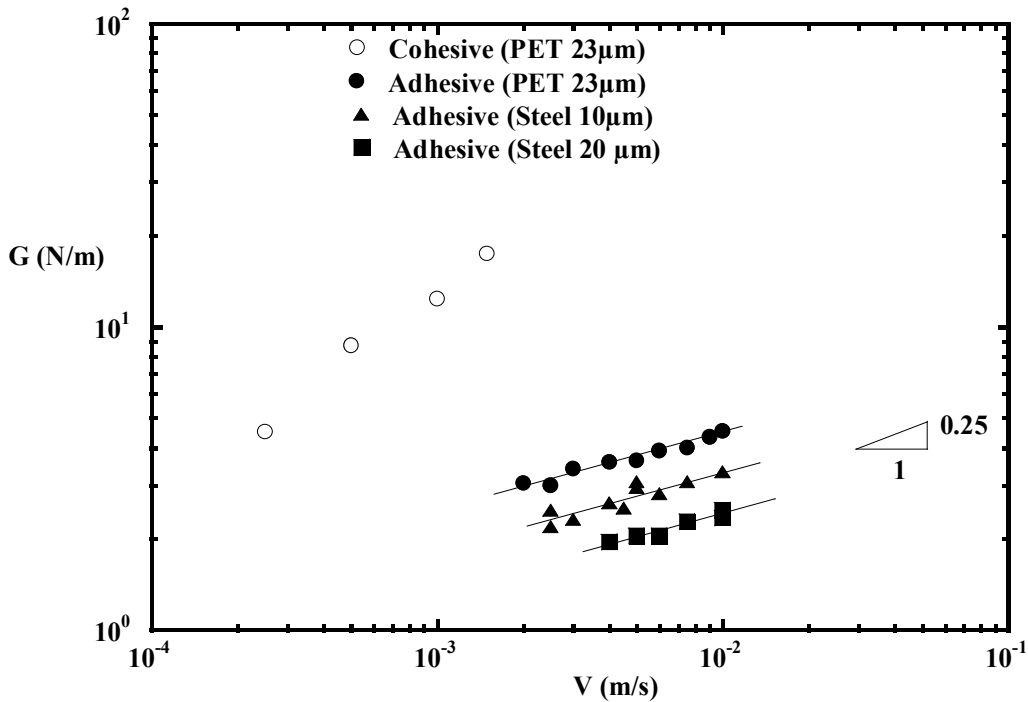


Figure 6. Peeling curve. Influence of the peeling velocity and backing rigidity ($T = 20 \text{ }^\circ\text{C}$, $e = 80 \mu\text{m}$)

From this curve, we deduce the influence of the backing rigidity EI. Figure 7 shows that the dependence is a power law with a negative slope of -0.2, in the regime of velocities and thicknesses studied.

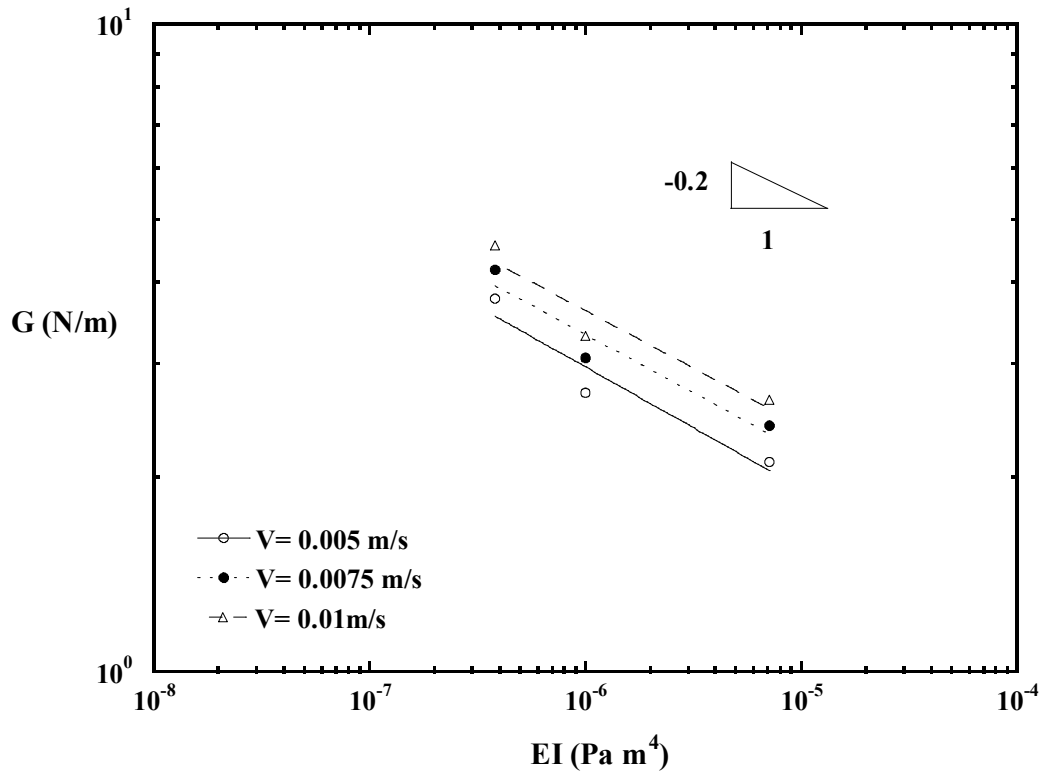


Figure 7. Influence of the backing rigidity for different velocities ($T= 20\text{ }^{\circ}\text{C}$, $e=80\text{ }\mu\text{m}$).

This result might seem unusual, but we may note that it is in agreement with Bikerman's formula²¹. To sum up these results, we finally we obtain the dependence of the energy of restitution rate G in terms of the three parameters V , e , and Eh^3 .

$$G \approx V^{0.25} e^{0.33} (Eh^3)^{-0.2} \quad (2)(2) \quad (4)$$

We will now try to explain these results in the next part.

THEORETICAL PEELING MODEL FOR A POWER LAW FLUID

To propose an explanation of the results previously obtained, we consider figure 8, as the starting sketch representing the locus of failure in the adhesive regime.

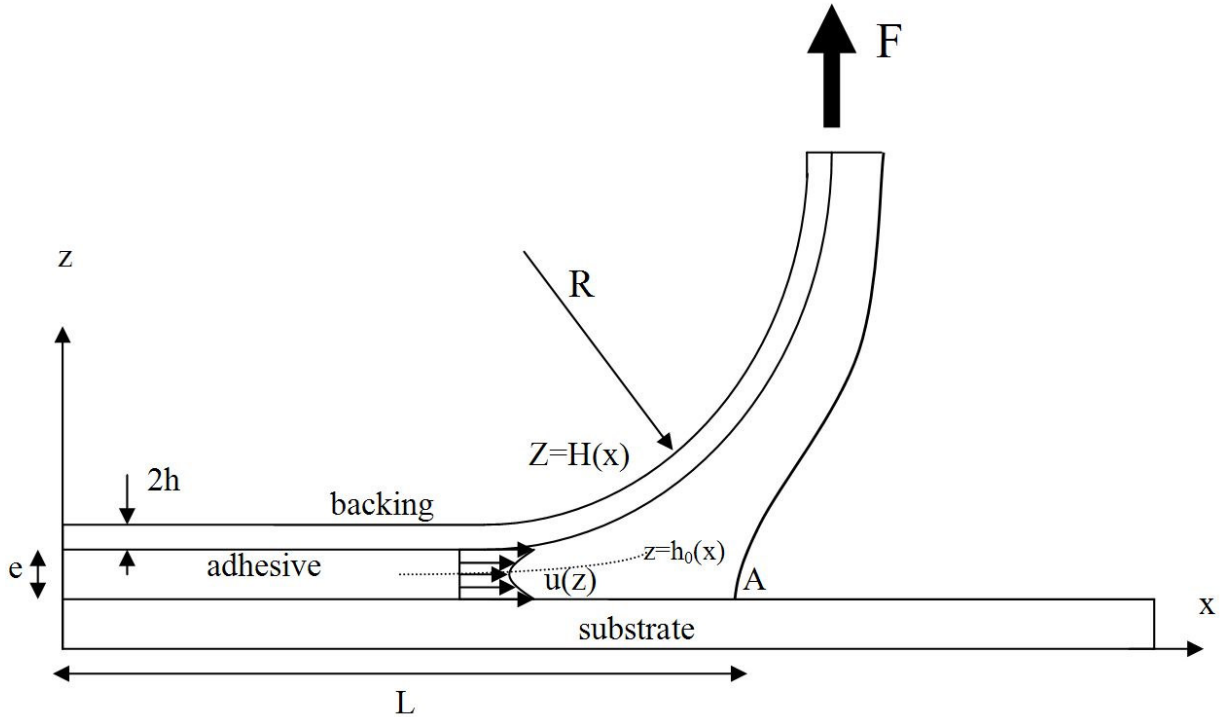


Figure 8. Sketch of the adhesive regime of failure. $Z=H(x)$ is the backing shape. $u(z)$ is the x -component of the velocity field. The velocity gradient $\frac{du}{dz}$ is > 0 or < 0 depending on z . $z=h_0(x)$ is the critical line where $\frac{du}{dz} = 0$. L is a typical length scale of the region of deformation.

The adhesive is brought to the contact failure zone (point A) where it detaches from the substrate. During such a motion, the flow of the adhesive can be considered, according to lubrication theory, to be a homogeneous flow with its major component $\mathbf{u} = u(z) \mathbf{e}_z$, where \mathbf{e}_z is a unit vector. According to lubrication theory, the z -component of the momentum equation is written by

$$-\frac{dp}{dx} = \frac{\partial \sigma_{xz}}{\partial z} \quad (5)$$

where p is the pressure and σ_{xz} the relevant shear component. Equation (5) can be integrated

$$\sigma_{xz} = -A(x)z + B(x) \quad (6)$$

where $A(x) = -\frac{dp}{dx} < 0$ is the non-zero pressure gradient, and $B(x)$ a function of x to be determined. We follow the analysis carried out in previous work¹⁰ but we use a power-law relationship for the fluid²², i.e.

$$\sigma_{xz} = m \dot{\gamma}^n \quad (7)$$

where $\dot{\gamma}$ is the shear rate (s) (taken >0 here), n is the rheofluidification fraction exponent, typically $0 < n < 1$, and m is a constant. This will allow to obtain different adhesive behaviours according to the power-law index n . Depending on the shear rate, the viscosity curve $\eta = m \dot{\gamma}^{n-1}$ exhibits an exponent $n \approx 1$ at low shear rates, and a value of n of the order $n \approx 0.4$ at the higher shear rates, by inspection of figure 1.

The shear rate $\dot{\gamma}$ is determined by $\dot{\gamma} = \left| \frac{du}{dz} \right|$ since $\frac{du}{dz}$ can be positive or negative according to this relation. There is a critical line $z = h_0(x) = \frac{B(x)}{A(x)}$ (see figure 8), below which $\frac{du}{dz} < 0$, and above which $\frac{du}{dz} > 0$. Accordingly, the solution of (6)-(7) will be divided into two parts, to

preserve the correct signs:

$$\bullet \quad z < h_0(x) \quad m \left(-\frac{du}{dz} \right)^n = B(x) - A(x)z \quad (8)_a$$

$$\bullet \quad z > h_0(x) \quad m \left(\frac{du}{dz} \right)^n = A(x)z - B(x) \quad (8)_b$$

The solution of (5) can easily be obtained and the integration yields:

$$\bullet z < h_0(x) \quad u^-(z) = \frac{m}{A} \frac{1}{\frac{1}{n} + 1} \left(\frac{B - Az}{m} \right)^{1/n+1} + C^-(z) \quad (9)_a$$

$$\bullet z > h_0(x) \quad u^+(z) = \frac{m}{A} \frac{1}{\frac{1}{n} + 1} \left(\frac{Az - B}{m} \right)^{1/n+1} + C^+(z) \quad (9)_b$$

$C^-(z)$ and $C^+(z)$ are integration constants to be determined.

Using the proper boundary conditions, i.e., $u^-(0) = V$, $u^+(H) = V$, $u^-(h_0) = u^+(h_0)$ and

$$\frac{du^-}{dz}(h_0) = \frac{du^+}{dz}(h_0) = 0 \text{ (this last one is satisfied because it corresponds to the critical line where}$$

$\dot{\gamma} = 0$), we obtain the unknown constants $C^-(z)$, $C^+(z)$ and $h_0(x)$:

$$C^-(z) = C^+(z) = V - \frac{m}{A} \frac{1}{\frac{1}{n} + 1} \left(\frac{AH}{2m} \right)^{\frac{1}{n} + 1} \quad (10)$$

$$h_0(x) = \frac{H(x)}{2} \quad (11)$$

We note here that the line for which the shear rate changes sign corresponds to the “mid-line”

$\frac{H(x)}{2}$ between the substrate and the backing. We next compute the flow rate Q :

$$eV = Q = \int_0^{H(x)} u(z) dz = \int_0^{H(x)/2} u^-(z) dz + \int_{H(x)/2}^{H(x)} u^+(z) dz \quad (12)$$

After a few simplifications, the integration is used to obtain the pressure gradient:

$$A(x) = -\frac{dp}{dx} = \frac{2m}{H} \left(\frac{2V(H - e)}{H^2} \frac{2n + 1}{n} \right)^n \quad (13)$$

This result can be checked with previous work¹⁰, where it was found that $\frac{dp}{dx} = -\frac{12\eta V(H-e)}{H^3}$,

in agreement with the Newtonian behaviour corresponding to the limiting case $m=\eta$ and $n=1$.

The pressure drop across a typical length scale L (see figure 8) is now expressed by:

$$\Delta p = \int_0^L \frac{dp}{dx} dx = \int_0^L -\frac{2m}{H} \left(\frac{2V(H-e)}{H^2} \frac{2n+1}{n} \right)^n dx \quad (14)$$

This integral can only be evaluated when a typical function is used for $H(x)$. In the present analysis, we use:

$$H(x) = e + \frac{x^2}{2R} \quad (15)$$

where R is a radius. This radius is in fact the initial radius of curvature R (for $x=0$), and can be measured in our experiments, as seen for example in figure 9. Further careful analyses of the shape of the backing confirms that this shape is in very good agreement with experimental data¹⁶.

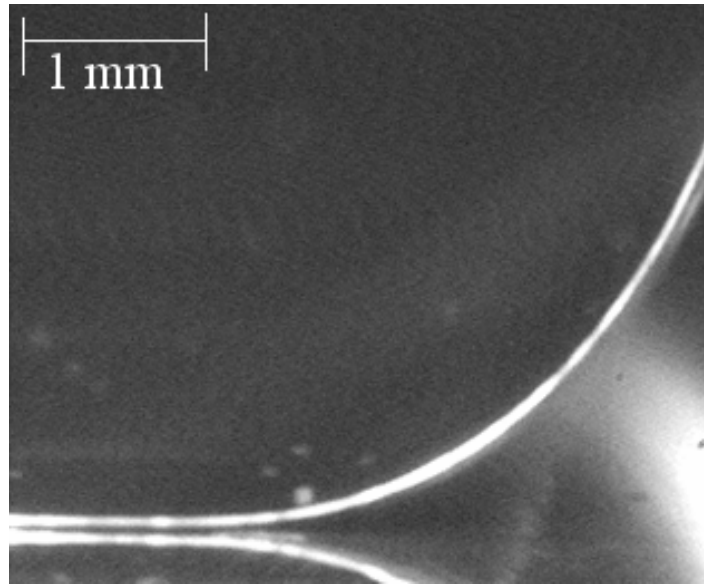


Figure 9. Shape of backing showing initial radius of curvature R (stainless steel, $2h=10 \mu\text{m}$).
 $V=10^{-2}$ m/s. $T=20^\circ\text{C}$

Finally, equation (14) can be integrated formally, using Matlab™, and the result is found to yield the following scaling laws, provided that $L > \sqrt{eR}$, which is satisfied in our experiments (typically $R=2\text{mm}$, $e=80\mu\text{m}$, and $L=2\text{mm}$, so $\sqrt{eR} \approx 0.4\text{ mm}$)

$$\Delta p \approx m \left(\frac{V}{e} \right)^n \sqrt{\frac{R}{e}} \quad (16)$$

Again, these results are checked with a previous analysis¹⁰ where it was found that $\Delta p \approx \eta \frac{V}{e} \sqrt{\frac{R}{e}}$ for a Newtonian adhesive ($n=1$, $m=\eta$). The influence of the shear-thinning index n is therefore demonstrated to act through the power n of a typical shear rate $\frac{V}{e}$. Proceeding further, the pressure is assumed to match the force applied at the ends of the ribbon, after considering the geometry of a small beam element:

$$\Delta p b R = F \quad (17)$$

where b is the bond width and F is the applied force measured in the experiments. The radius of curvature also appears and is taken to vary as $R \approx \sqrt{\frac{EI}{F}}$. Finally, we obtain:

$$\Delta p \approx m \left(\frac{V}{e} \right)^n \left(\frac{EI}{F} \right)^{1/4} \frac{1}{\sqrt{e}} \approx \frac{F^{3/2}}{b\sqrt{EI}} \quad (18)$$

This leads to the energy of restitution rate spent to peel the adhesive strip (using $I = \frac{2bh^3}{3}$):

$$\frac{F}{b} \approx m^{4/7} \frac{V^{4n/7}}{e^{(4n+2)/7}} (Eh^3)^{3/7} \quad (19)$$

This final result demonstrates the ability of the model to account for rheofluidification with index n , the case of the Newtonian fluid being recovered by setting $n=1$ and $m=\eta$ (the Newtonian viscosity).

In our experiment, the velocity ranges from $10^{-3} \text{ m/s} < V < 10^{-2} \text{ m/s}$, whereas the thickness is of the order of $100 \mu\text{m}$. The typical shear rate $\frac{V}{e}$ varies between 10 and 10^2 s^{-1} . This means, that,

referring to figure 1, the viscosity behaviour is like $\eta \approx m \dot{\gamma}^{-0.6}$, so n can be taken to be $n \approx 0.4$.

Inserting this into (19) leads to the relationship for the force per unit width:

$$\frac{F}{b} \approx V^{0.23} e^{-0.51} (Eh^3)^{0.43} \quad (20)$$

The model is therefore quite accurate for predicting the velocity dependence but fails to describe the behaviour in terms of the backing rigidity and adhesive thickness. Still it is helpful for putting the basis of a more careful analysis presented next.

DISCUSSION

Cohesive-adhesive transition

We first investigate the transition between cohesive and adhesive failure modes in figure 3. According to a previous study²³, elastic effects have been shown to play an important role in the deformation processes involved in probe-tack experiments, as suggested by the introduction of a Deborah number. At small Deborah numbers ($De < 1$), the viscous effects dominate, whereas for high Deborah numbers ($De > 1$), elasticity becomes important. Such effects (deformations) can be relevant here because mechanisms involved during probe-tack experiments are comparable to the ones in peel tests²⁴. We will rather introduce the Weissenberg number $Wi = \lambda V / e$ ($\lambda = 3 \text{ s}$, V is the velocity of peel, and e the adhesive thickness), as in our previous study⁸. This number is equivalent to the Deborah number described above²³. For the transition from cohesive to adhesive failure, inspection of figure 3 gives the following transition velocities $V_c = 0.5 \cdot 10^{-3} \text{ m/s}$, $1.5 \cdot 10^{-3}$

m/s, $4.0 \cdot 10^{-3}$ m/s corresponding to thicknesses of 40, 80, 160 μm . They correspond to the first unstable velocities of peel. In fact, in some cases, there is a wide region of instability. Such transition velocities can be related to the equivalent Weissenberg number. They correspond respectively to values of $W_i = 37.5, 56.2$ and 75 , slightly smaller than the ones found previously²³. According to this data, the transition velocity varies approximately with thickness (e) like a power law $e^{2/3}$. This is in favor of the idea that the Weissenberg number cannot alone distinguish between the cohesive and adhesive regimes, but may come out in combination with another dimensionless parameter like one based on surface energies⁸. Further studies are still needed to provide such evidence. In any case, the values found for the Weissenberg number are typical of an elastic behavior, and they fall in the range of the ones indicated previously²³ in the case of acrylic adhesives (between 100 and 1000 at the cohesive to adhesive transition). This enforces the fact that peel and tack experiments are clearly related.

Model for predicting interfacial failure

According to various authors, the peeling energy is closely related to the influence of the backing curvature^{21,25}, because the flow induced within the adhesive generates stresses, which conversely modify the backing curvature changing again stresses inside the adhesive; finally an equilibrium is found with a complex interdependence of all the parameters, as just shown above. In practice, Bikerman²¹ proposed with the following expression :

$$\frac{F}{b} = 0.4 \sigma_0 e^{0.25} h^{0.75} \left(\frac{E^*}{E} \right)^{0.25} \quad (21)$$

Where σ_0 is a typical stress, and E^* is the adhesive's Young modulus, when it is considered as a linear elastic solid. This expression also has the problem of the absence of velocity, and the wrong dependence on adhesive thickness (although better) and backing thickness. On the other

hand, the dependence on the adhesive modulus E is rather accurate (power law -0.25 instead of -0.2 in the experiments). This formula is difficult to use here and we will rather rely on the analysis from the previous part, based on the following ideas.

- 1) The correct dependence in terms of the velocity V (shown to be close to 0.25) has shown the relevance of the power law index n, which should be used for modelling adhesive stresses and viscosity.
- 2) Dimensional analysis⁸ shows the importance of the relevant numbers. The first one is the Weissenberg number for viscoelasticity W_i . Indeed, simple models using either viscous or elastic adhesives fail to describe the problem. The Weissenberg number W_i has been defined previously as :

$$W_i = \lambda \frac{V}{e} \quad (22)$$

ξ is the second dimensionless number accounting for the competition between curvature effects and viscous stresses. $\xi = \frac{\sigma e^3}{Eh^3}$ where σ is a typical stress within the adhesive. Here a

typical stress¹⁶ is $\sigma = m \dot{\gamma}^n = m \left(\frac{V}{e} \right)^n$, therefore

$$\xi = \frac{m \left(\frac{V}{e} \right)^n e^3}{Eh^3} \quad (23)$$

- 3) Finally the force per unit width $G=F/l$ will depend on these numbers in a combined manner, and we may look for a solution of the kind :

$$G = \frac{F}{l} \approx \xi^a W_i^b \quad (24)$$

Using $a=0.2$ takes care of the backing rigidity influence, and we are left with the effect of the velocity V and thickness effects. Choosing the velocity V , we need to insure from (4) and (24) that $an + b = 0.25$. Since $n=0.4$ from figure 1, we find that $b=0.13$. The power law dependence in terms of the adhesive thickness e is deduced to be $e^{(3-n)a-b} = e^{0.39}$, which gives a very nice comparison with experiments (slope 0.33). Finally, we find :

$$G = \frac{F}{l} \approx \xi^{0.2} W_i^{0.13} \approx \left[\frac{m \left(\frac{V}{e} \right)^n e^3}{Eh^3} \right]^{0.2} \left(\frac{\lambda V}{e} \right)^{0.13} = k V^{0.25} e^{0.39} (Eh^3)^{-0.2} \quad (25)$$

The dimensionless coefficient k in front of (25) has been found experimentally¹⁶ to be around $k=500$. This analysis has not taken into account the surface energy properties, since one substrate (HDPE) and one adhesive only were used, therefore (25) does not contain the surface energy parameters. Following the work of Gent and Schultz¹² and other authors^{13,14,15}, we suggest a possible extension of the model in terms of the surface parameters, in particular the Dupré work of adhesion W_a :

$$G = \frac{F}{l} = W_a (1 + k \xi^a W_i^b) \quad (26)$$

The parameters k , a and b are very likely to be different depending on the adhesives. In our case, for the present adhesive (PDMS), in the range of parameters used (velocity of peel, thickness, backing rigidity), we found that $k \approx 500$, $a=0.2$ and $b=0.13$. Note that the Dupré work of adhesion W_a might, in some cases, be replaced by other modified expressions, as suggested in previous works^{5,13}. To summarize, this analysis is based on the shear rheological properties of the adhesive only and is therefore relevant to the linear PDMS polymer studied here, but would need to be modified when elongational effects become relevant (branched polymer adhesives²³, or strain

hardening materials, as in previous studies^{2,7-8}). This would probably affect the values of the parameters k , a and b determined above.

CONCLUSIONS

In the present analysis, it has been shown that modelling the peeling behaviour of viscoelastic adhesives is still a challenge. After obtaining peeling data corresponding to a variety of parameters, it has been shown that the competition between backing rigidity and viscous behaviour is of importance, as shown in previous studies^{10,21}, and leads to the introduction of a dimensionless parameter ξ , modified to take into account the shear-thinning behaviour of the adhesive. A detailed analysis showed indeed that the peeling force model predicts very well the velocity dependence when a power-law fluid dependence is used. This non-Newtonian effect is typical of the most common adhesives.

On the other hand, to predict correctly the dependence of the peel force in terms of adhesive thickness and backing rigidity, an empirical model has been proposed, based on the use of another dimensionless number for viscoelasticity, the Weissenberg number W_i . Although the peel force depends slightly on W_i (small power law exponent), it is necessary to introduce it in order to derive a correct description of the results for viscoelastic adhesives^{5,13}.

ACKNOWLEDGMENTS

The authors are grateful to N. El Kissi for providing the PDMS adhesive as well as its rheometrical properties.

REFERENCES AND NOTES

1. Kaelble, D. H. *Trans Soc Rheol* 1959, 3, 161–180.
2. Benyahia, L. ; Verdier, C. ; Piau, J.-M. *J Adhesion* 1997, 62, 45-73.
3. Zosel; A. *Coll Polym Sci* 1985, 263, 541-553.
4. Lakrout, H.; Sergot, P.; Creton, C. *J Adhesion* 1999, 69, 307-359
5. Deruelle, M.; Léger, L.; Tirell, M. *Macromolecules* 1995, 28, 7419–7428.
6. Roos, A. ; Creton, C. ; Novikov, M.B. ; Feldstein, M.M. *J Polym Sci Part B: Polym Phys* 2002, 40, 2395-2409.
7. Verdier, C. ; Piau, J.-M. ; Benyahia, L. *C. R. Acad. Sci. Paris, Série Iib* 1996, 323, 739-746.
8. Piau, J.-M.; Verdier, C. ; L. Benyahia, L. *Rheol Acta* 1997, 36(4), 449-461.
9. Connelly, R.W.; Parsons, W.F.; Pearson, G.H. *J Rheol* 1981, 25, 315-328.
10. Piau, J.-M.; Ravilly, G ; Verdier ; C. *J Polym Sci Part B: Polym Phys* 2005, 43, 145-157.
11. Urahama, Y. *J Adhesion* 1989, 31, 47-58.
12. Gent, A. N.; Schultz, J. *J Adhes* 1972, 3, 281–294.
13. Carré, A.; Schultz, J. *J Adhes* 1984, 17, 135–156.
14. Andrews, E.H.; Kinloch, A.J. *Proc R Soc London A* 1973, 332, 385-399.
15. Andrews, E.H.; Kinloch, A.J. *Proc R Soc London A* 1973, 332, 401-414.
16. Ravilly, G. Ph.D Thesis, Adhésion et pelage bidimensionnel des polymères, Université de Grenoble I, Grenoble, France, february 2001.
17. El Kissi N. ; Piau, J.-M. ; Attané, P.; Turrel, G. *Rheol. Acta* 1993, 32, 293-310.
18. Mestadi, A. Ph.D Thesis, Caractérisation en élongation de polymères fondus et en solution : comparaison entre essais à force constante et à vitesse de déformation constante, Université de Grenoble I, Grenoble, France, july 1995.
19. Owens, D. K.; Wendt, R. C. *J Appl Polym Sci* 1969, 13, 1741-1747.

20. van Oss, C. J.; Giese, R.F.; Wu, W. *J Adhesion* 1997, 63, 71-88.
21. Bikerman, J. J. *J Appl Phys* 1957, 28, 1484–1485.
22. Bird, R. B. ; Armstrong, R. C. ; Hassager O. In *Dynamic of polymeric liquids. I. Fluid Mechanics*, Wiley: New York, 1987 (2nd edition); Chapter 6.
23. Lakrout, H. ; Creton, C. ; Ahn, D. ; Shull, K.R. *Macromolecules* 2001, 34, 7448-7458.
24. Verdier, C.; Piau, J.M. *J Polym Sci Part B: Polym Phys* 2003, 41, 3139-3149.
25. Niesiolowski, F.; Aubrey, D. W. *J Adhes* 1981, 13, 87–98.